Impact of Varying Ground Control Points Configurations on the Accuracy of Unmanned Aerial Vehicle-Based Digital Elevation Models

Benito, C. A.[1, 2*] and Opon, J. G.[3,4]
[1]Graduate School of Engineering, College of Engineering, Mindanao State University-Iligan Institute of Technology, 9200 Philippines
[2]Department of Civil Engineering, College of Engineering and Information Technology, University of Southern Mindanao, 9407 Philippines, E-mail: cabenito@usm.edu.ph*
[3]Center for Structural Engineering and Informatics, Research Institute for Engineering and Innovative Technology, Mindanao State University-Iligan Institute of Technology, 9200 Philippines
[4]Department of Civil Engineering and Technology, College of Engineering, Mindanao State University-Iligan Institute of Technology, 9200 Philippines, E-mail: joel.opon@g.msuiit.edu.ph
**Corresponding Author*

DOI: https://doi.org/10.52939/ijg.v20i11.3705

Abstract
Ensuring the vertical and horizontal accuracy of UAV-DEM is crucial for precision of results in any geohazard modeling like flood modeling. Various factors affecting UAV-DEMs accuracy, particularly the number and spatial distribution of Ground Control Points (GCPs) used in the surveyed area. This study aimed to identify the most effective GCP configuration for the UAV-DEM by assessing its impact on the vertical and horizontal accuracy of UAV-DEMs, considering GCP configurations involving different numbers (4, 8, 12, 16, and 20) and distributions (Outer, Center, and Stratified). The investigation employed a Factorial Experimental Design with three replications. The results revealed that UAV-DEMs with 8, 12, 16, and 20 GCPs exhibited higher vertical accuracy compared to those with 4 GCPs. While 4, 8, 12 and 16 number of GCPs will have the same effect on the horizontal accuracy. Additionally, both outer and stratified distributions surpassed center distribution for both vertical and horizontal accuracy. Furthermore, the study produced 20-cm Vertical Accuracy Class with 10-cm Horizontal Accuracy class based on ASPRS Positional Accuracy Standards for Digital Geospatial Data of 2023. Consequently, the study recommends an optimal GCP configuration involving 8 GCPs with either Outer or Stratified Distribution for every 100-hectare (1 km^2) study area.

Keywords: Digital Elevation Model, Ground Control Points, Horizontal Accuracy, Unmanned Aerial Vehicle, Vertical Accuracy

1. Introduction

The emergence of geographic information systems (GIS) and geohazard computer models has elevated the significance of digital elevation model (DEM) as highly important and effective tools in various environmental applications, such as flood modeling [1] and [2]. Understanding and predicting flood behavior is crucial, and use of DEMs for flood modeling serves this purpose [3]. The DEM depicts the actual surface of the earth and aids in understanding the attributes of the terrain [4]. Precise and detailed DEMs are essential to accurately predict floods [5]. However, with decreasing DEM accuracy and resolution, the predicted flood inundation areas could result in over-predicting the flood extent [6].

In many countries, especially for small river basins, no accurate DEMs have been developed and continue to depend on elevation data obtained from space based DEMs [7]. The utilization of airborne light detection and ranging (LiDAR) systems has emerged as an effective method for generating DEMs, offering the advantage of efficiently capturing three-dimensional information across expansive areas with precision and speed [8]. LiDAR DEM resolves terrain with the accuracy of vertical RMSE of 5-20 cm [9]. However, a notable drawback of using manned aerial platforms like airplanes is their high cost, particularly when dealing with smaller study areas [10].

Therefore, the commonly used DEMs are based on globally available datasets like advanced spaceborne thermal emission and reflection radiometer (ASTER) and shuttle radar topography mission (SRTM) [9] [11] and [12]. Assessment study of these open-sourced elevation data sets found a very high vertical error of 5.68 m up to 11.98 m [11]. Inaccuracies in vertical elevation can impact the precision of terrain simulation, consequently influencing flooding simulation accuracy as well [13] and [14]. Accurate DEMs are essential for achieving high precision flood modeling [15]. In lieu of other methods to generate DEMs, unmanned aerial vehicles (UAVs) are often used for generating elevation datasets to create more accurate DEMs. UAV, commonly known as drone, is a robotic airborne system that operates either remotely or autonomously using onboard sensors and global positioning system (GPS) to execute flight maneuvers guided by software control. Drones are also being used in different applications such as in architecture, construction, design, monitoring, mapping, and remote sensing [16][17] and [18].

The advancement of UAVs and photogrammetric processing software has created a new platform for a low-cost UAV-based digital elevation model (DEM) for remote sensing of geological hazards. These platforms have the capability to acquire extremely detailed (centimeter-level) imagery and create dense point clouds, allowing for the cost-effective generation of DEMs [19][20] and [21]. Nevertheless, the UAV-based DEMs exhibit an average elevation accuracy ranging from 3.1 to 3.3 meters (RMSE), with an average horizontal accuracy of 2.1 meters [22]. This error rate remains excessively high to be used as elevation datasets. As such, it is essential to maintain accuracy in UAV photogrammetry within acceptable parameters [23] and [24]. Numerous variables influence the accuracy of UAV photogrammetry, e.g., flight planning, camera specifications, structure from motion (SfM) algorithms, and ground control points (GCPs) configuration [25]. Among these factors, the impact of the georeferencing approach (ground control points configurations) holds particular importance, especially the quantity and spatial distribution of ground control points. Georeferencing involves aligning the outcomes of bundle adjustment and photogrammetric procedures with a particular coordinate system [26].

The extant literature has provided recommendations regarding the optimal GCPs configurations to be used in various scenarios to produce accurate DEMs. According to previous studies, GCPs should be positioned at a density ranging from 0.5 to 3 GCPs per hectare [24] and [27], with some recommendations suggesting one GCP per 2 hectares [28]. The best distribution are the edge and stratified distributions [24], while an evenly distributed set has also been demonstrated to be effective [29]. Additionally, stratified random allocation can be employed to position GCPs across the study area to ensure accurate coverage [30]. The mentioned works consistently shows that accuracy of DEMs enhances with an increasing number of GCPs, reaching an asymptotic trend rapidly [24][29][31] [32] and [33].

However, deploying GCPs in the field, conducting surveys, and identifying them in images can be a time-consuming and costly endeavor [34]. Furthermore, the process of measuring the coordinates of the GCPs can be labor-intensive and occasionally challenging due to the topographical characteristics of the terrain [24]. As a result, there may be situations where the ideal GCPs configuration cannot be put into practice in real projects. Exploring how varying the number and distribution of GCPs impacts UAV-DEMs accuracy provides insights into determining the best GCPs configuration for different field scenarios. Achieving high DEMs accuracy is crucial, as it enhances the capability to estimate inundation areas and assess the associated flood modeling risks more effectively [35]. Along with this vein, it is the objective of this paper to present optimum number and spatial distribution of GCPs that could yield acceptable level UAV- DEM vertical and horizontal accuracy.

2. Methodology

The workflow of this study, illustrated in Figure 1, follows a structured approach to assess the effect of different GCPs configurations on the accuracy of UAV-based DEMs.

2.1 Study Area

The study area is situated along a portion of the floodplain of the Mandulog River in Iligan City, Lanao Norte, Philippines (Figure 2). The designated area exhibited persistent flooding, particularly during the severe incident on December 17, 2011, when Typhoon Sendong struck, leading to the tragic loss of 490 lives. It is located at a latitude of 8.25° N and a longitude of 124.26° E. The longitudinal orientation of the site spans from east to west, covering a distance of approximately 2.0 km, while the latitudinal direction extends from north to south, covering a distance of around 0.7 km. The study area encompasses an approximate area of 1.0 square kilometer (km^2) or 100 hectares (ha).

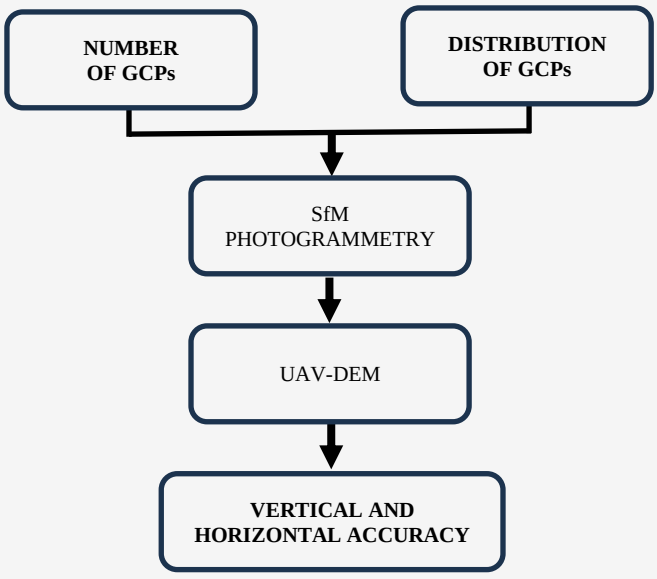

Figure 1: Study workflow

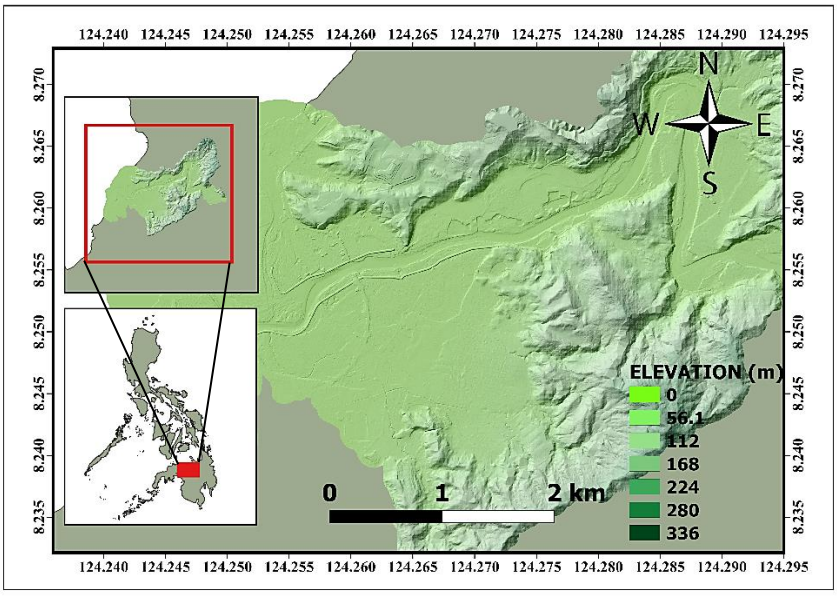

Figure 2: Lanao Norte, the Philippines

The chosen study area includes diverse land uses such as residential, commercial, industrial, recreational, and transportation. This configuration is representative of typical scenarios encountered in urban UAV projects, encompassing both artificial surfaces like roofs, facades, parking lots, and roads, as well as natural surfaces like green areas. Frequently, the natural environment poses challenges or renders it unfeasible to place GCPs and checkpoints (CPs) [30].

2.2 Acquisition of Photogrammetric Data

Photogrammetric data was acquired utilizing the Skywalker 1900 mm fixed-wing UAV, with a wingspan of 1900 mm, a length of 1300 mm, a flying weight of 2.4 kg equipped with 2 x 14.8 v 5000 mAh batteries and a camera. This UAV is capable of a maximum flight time of 1 hour and 50 minutes. The image capture was executed with a Sony RX100 camera, a 20.2-megapixel camera featuring a global shutter, a fixed focal length of 10.4 mm, and an aperture of F2.8. Table 1 shows the specifications of the UAV and camera. Mission planning and control for the flight were executed through Mission Planner version 1.3.6777.19762 and was 120 m above ground level. The percentages of side and front overlaps were set at 80% and 80%, respectively.

Table 1: UAV and Camera Specifications.

Drone: Skywalker 1900	
Wingspan	1900 mm
Length	1300 mm
Flying Weight	2.4 kg
Battery	2 x 14.8 v 5000 mAh
Flight Time	1 hr and 50 minutes
Camera: Sony RX100	
Camera Resolution	20.2 MP
Focal Length	10.4-37.1 mm
Lens Aperture	f/1.8-f/4.9
Maximum Shutter Speed	1/2000 sec
Continuous Shooting Speed	10 fps
Size	102 x 58 x 36 mm

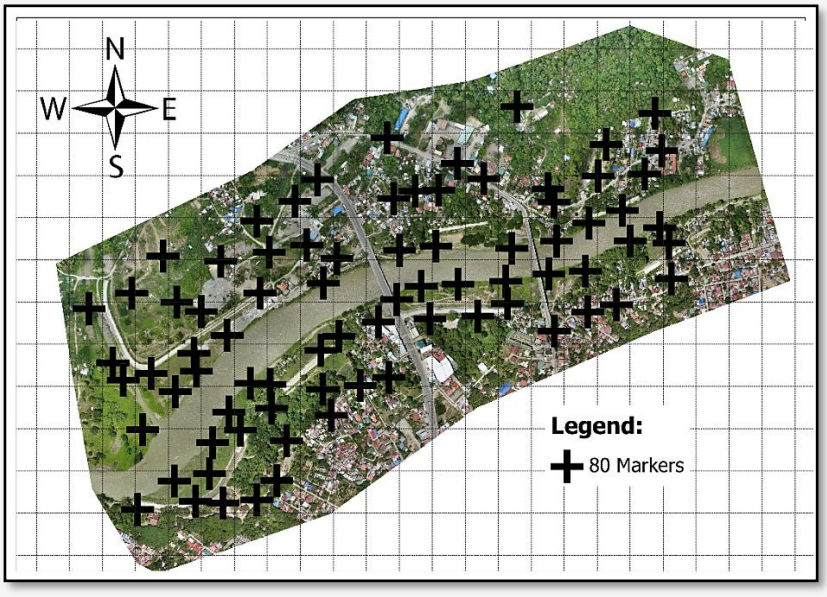

Figure 3: Ground markers

The flight plan specified a constant horizontal ground speed of 2.5 meters per second, and images were taken at 2-second intervals either near or directly beneath the observation point (nadir). The flight path consisted of parallel lines with an estimated coverage area of 486 by 365 meters, and total of 2, 663 images were processed. The resulting ground sample distance (GSD) of the study is 4.93 cm.

2.3 Ground Markers

Prior to acquiring photogrammetric data, ground markers were placed throughout the study area to function as GCPs and CPs, which were subsequently employed to assess the accuracy of the UAV-DEMs. Since the study area has mixed land use, such as residential areas, it is difficult to place uniformly spaced markers. The placement of ground markers depends on a grid created with an approximate size of one hectare each, with the researcher placing a single ground marker within each hectare [24]. The placement of markers is done in the most suitable location if it fits within the defined grid. Figure 3 shows the locations of the ground markers. The 3-D coordinates of this ground markers were determined using South Galaxy G7 Plus GNSS-RTK base and rover incorporating differential corrections.

2.4 Experimental Set-up

GCPs configurations were varied following a Factorial Experimental Design as shown in Figure 4, incorporating two independent variables: 1) The Number of GCPs: 4, 8, 12, 16 and 20; and 2) Distribution of GCPs: Outer, Center, and Stratified. Each experimental setup was replicated three times. Additionally, a Tukey post hoc test was conducted to further test the significant differences of vertical and horizontal accuracies. Figure 4 shows the combination of GCPs and CPs configuration.

GCPs Numbers	GCP distribution		
	Outer	Center	Stratified
4	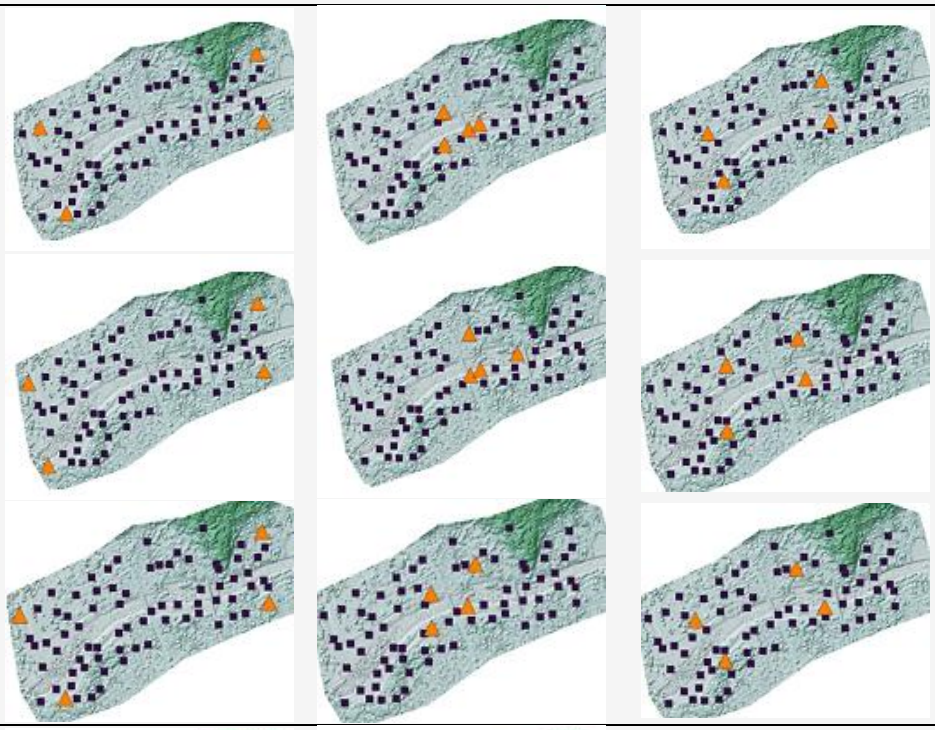		
8	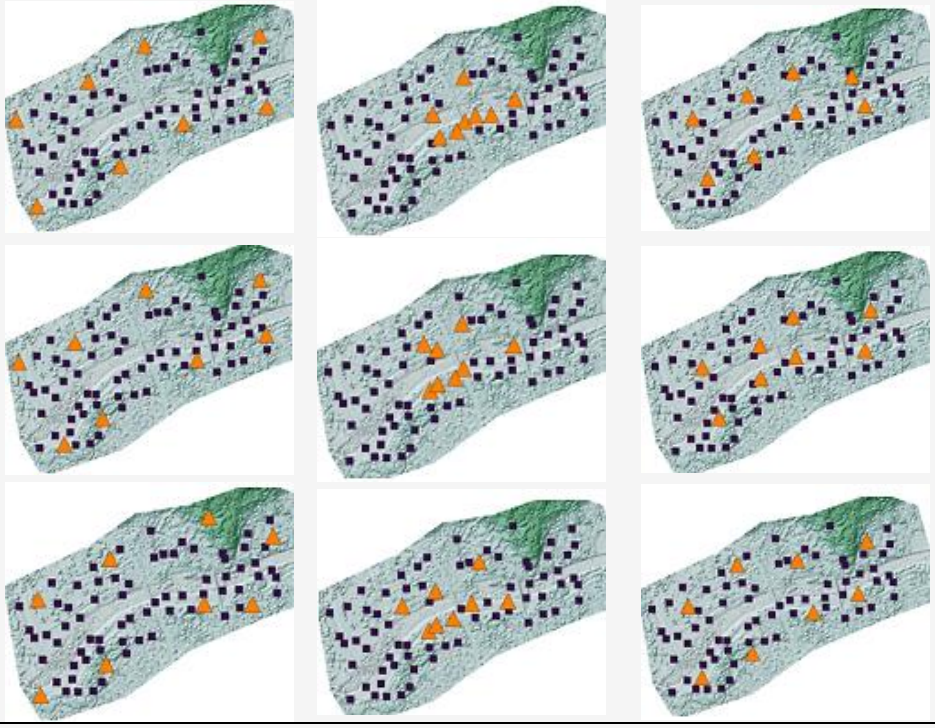		

Figure 4: GCPs and CPs configuration (Continue next page)

GCPs Numbers	GCP distribution		
	Outer	Center	Stratified
12	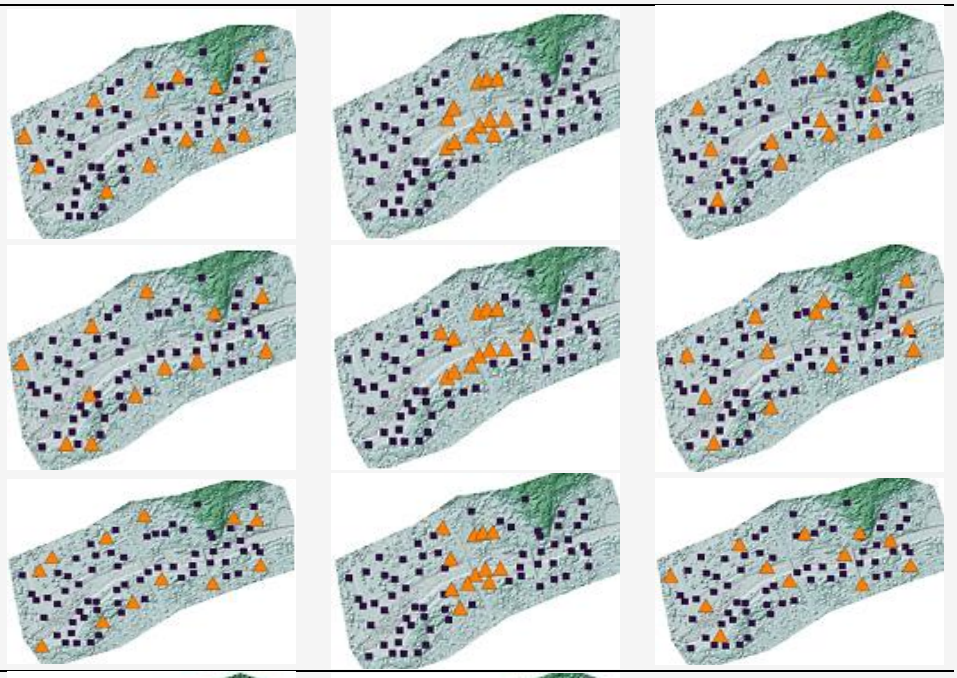		
16	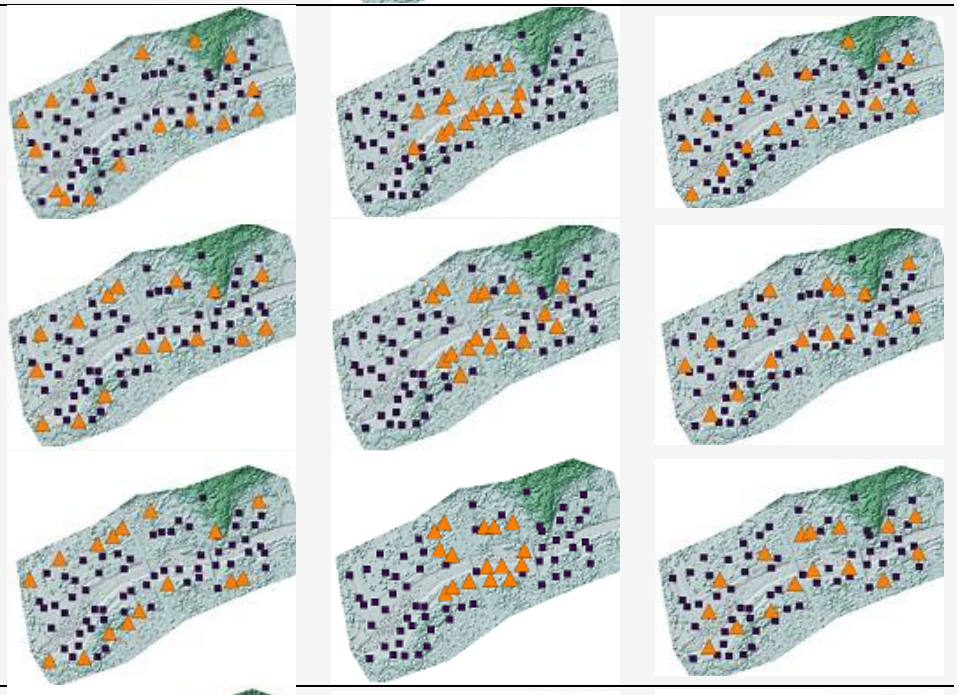		
20	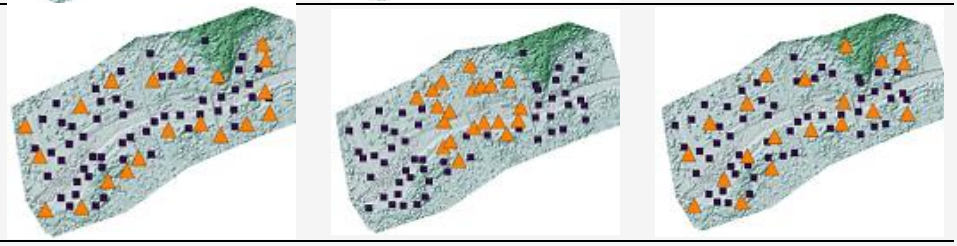		

Figure 4: GCPs and CPs configuration (Continue from previous page)

GCPs Numbers	GCP distribution		
	Outer	Center	Stratified
20	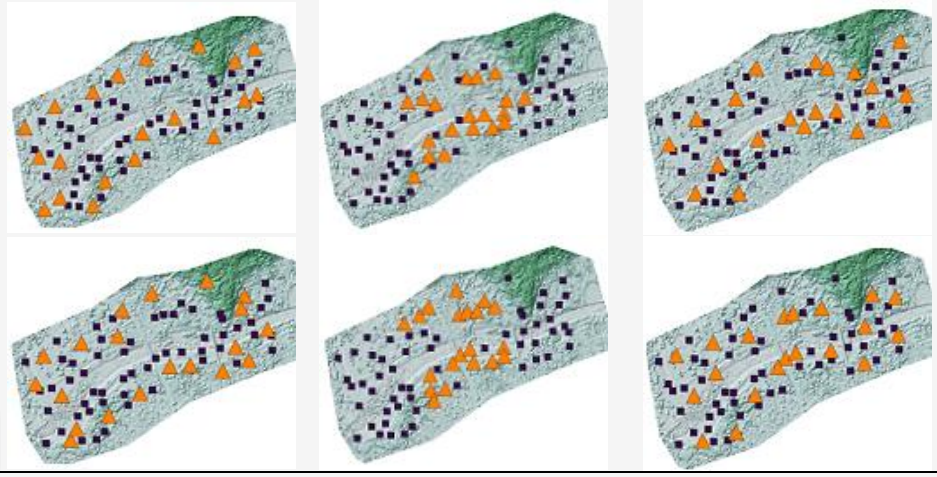		

Figure 4: GCPs and CPs configuration (Continue from previous page)

2.5 Photogrammetric Processing

The photogrammetric processing employed Pix4Dmapper version 4.4.4 software. The workflow comprises three primary steps [36]. In the initial phase, image alignment occurs through the identification and matching of features. The software then estimates camera orientation parameters. Out of the 2,663 images captured in the study area, only 2,659 images were successfully aligned as some photos failed to align because of poor quality or insufficient overlap. In the subsequent phase, the point cloud is tied up to the local coordinate system (WGS 84 and frames in UTM Zone 51N), and densification is achieved. This enhances the detail of the point cloud, resulting in a more intricate 3D model. The average dense cloud points per variation is approximately 580,709,000 with an average processing time of 8 hours and 16 minutes. In the third phase, texture is applied to the mesh obtained in the preceding step. Following this, the orthophoto is exported, and a grid DEM can be generated from the point cloud.

2.6 Accuracy Analysis

The Positional Accuracy Standards for Digital Geospatial Data Edition 2, Version 1.0 of 2023, published by the American Society of Photogrammetry and Remote Sensing (ASPRS) are designed to be adopted by both producers and users of geospatial data. This standard (ASPRS Edition 2, 2023) provides ten common vertical accuracy classes (Table 2). Vertical accuracy is to be expressed as $RMSE_V$ in both vegetated (VVA) and non-vegetated terrain (NVA). It is essential to explicitly define and report the horizontal accuracy ($RMSE_H$) of elevation data, classifying it according to the ASPRS Edition 2 (2023) standard, as outlined in Table 3.

Table 2: Vertical accuracy classification by ASPRS 2023

Vertical Accuracy Class	Absolute Accuracy	
	NVA $RMSE_V$ ≤ (cm)	VVA $RMSE_V$ (cm)
1.0	1.0	As found
2.5	2.5	
5.0	5.0	
10.0	10.0	
15.0	15.0	
20.0	20.0	
33.3	33.3	
66.7	66.7	
100.0	100.0	
333.3	333.3	

Table 3: Horizontal accuracy classification by ASPRS 2023

Horizontal Accuracy Class	$RMSE_H$ (cm)
0.6	0.6
1.3	1.3
2.5	2.5
5.0	5.0
7.5	7.5
10.0	10.0
12.5	12.5
15.0	15.0
17.5	17.5
20.0	20.0

Accuracy determination should align with project requirements, or it can be negotiated between data producers and clients. Specific accuracy thresholds and methods should be established based on the technology employed and the project design [37]. Accuracy evaluation was conducted by examining CPs, which are ground markers surveyed independently of those used for GCPs. This process entailed identifying the coordinates of CPs in the UAV-based DEM and Orthomosaic map and comparing their coordinates with the surveyed GNSS-RTK coordinates. The $RMSE_V$ and $RMSE_H$, are vertical and horizontal accuracies, respectively, which are defined in Equations 1 and 2:

$$RMSE_V = \sqrt{\frac{\sum_{i=1}^{n}\left(Z_i - Z_{RTKi}\right)^2}{n}}$$

Equation 1

$$RMSE_H = \sqrt{\frac{\sum_{i=1}^{n}\left[\left(X_i - X_{RTKi}\right)^2 + \left(Y_i - Y_{RTKi}\right)^2\right]}{n}}$$

Equation 2

Where:

Z_i = UAV-DEM derived elevation
Z_{RTKi} = RTK-GNSS derived elevation
X_i and Y_i = the horizontal coordinates
X_{RTKi} and Y_{RTKi} = the horizontal coordinates measured with RTK-GNSS
n = the total number of CPs

3. Results and Discussion

3.1 Vertical Accuracy

This study was performed to evaluate the effects of number of GCPs and spatial distribution of GCPs on the vertical accuracy of UAV-based DEM. Table 4 shows the data set of vertical accuracy in 5 x 3 factorial design of experiment with 5 level of number of GCPs and 3 levels of distribution of GCPs. The normality of the vertical accuracy data was determined by creating the Q-Q plot as in Figure 5. The figure reveals that the normality assumption is not met for vertical accuracy, hence data transformation is necessary. The configuration of the plot in Figure 5 showcases deviations at specific points, providing sufficient evidence to assert that the normality assumption is violated in this instance. Moreover, Table 5 presents the results of normality tests conducted using Kolmogorov-Smirnov and Shapiro-Wilk methods. Given the p-values (<.001) from both tests, we reject the null hypothesis asserting no difference between the anticipated normal distribution and the distribution of vertical accuracy. This implies that the data does not follow a normal distribution.

Table 4: Vertical accuracy

Number of GCPs	Vertical accuracy (cm)		
	Outer	Center	Stratified
4	157.30	172.80	174.20
	175.10	162.60	168.80
	175.12	161.20	160.00
8	21.40	128.90	22.30
	18.00	127.50	20.00
	23.00	96.60	16.40
12	29.70	151.20	18.80
	14.10	115.70	12.90
	30.70	135.40	12.90
16	11.60	55.50	11.50
	10.40	51.40	11.60
	13.70	82.60	11.70
20	10.00	72.50	10.70
	11.50	74.70	14.40
	13.10	72.70	12.60

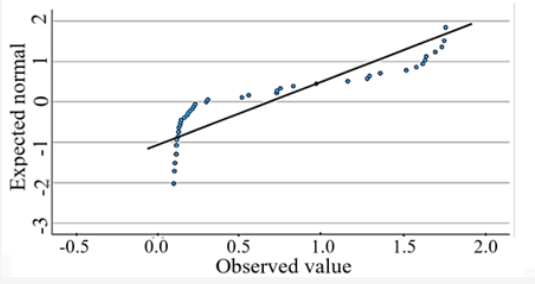

Figure 5: Normal Q-Q plot of vertical accuracy

Table 5: Test of normality before data transformation

	Kolmogorov-Smirnov			Shapiro-Wilk		
	Stat.	df	Sig.	Stat.	df	Sig.
Vertical Accuracy	.254	45	<.001	.788	45	<.001

Therefore, we can conclude that there is a need for transformation. Box-cox transformation was done in this study. Once the transformation of the data has been done, the normality of the data transformation was again verified. In Figure 6, it is evident that the plot exhibits an almost linear pattern, suggesting a normal distribution after transformation. The test of normality by Kolmogorov-Smirnov and Shapiro-Wilk was shown in Table 6, it can affirm here that the data transformation satisfies the assumption of normal distribution.

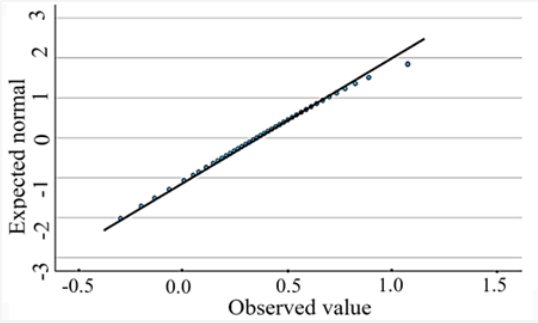

Figure 6: Normal Q-Q Plot of transformed vertical accuracy

Table 6: Test of normality after data transformation

	Kolmogorov-Smirnov			Shapiro-Wilk		
	Stat.	df	Sig.	Stat.	df	Sig.
Vertical Accuracy	.032	45	.200	.991	45	.982

Then, a two-way ANOVA was performed to evaluate the effects of number and distribution of GCPs on vertical accuracy of the UAV-based DEM. The means and standard deviations for transformed vertical accuracy of the UAV-DEM are presented in Table 7. In Table 8, the results indicated significant main effect of number of GCPs, F (4, 45) = 47.364, p = <.001, partial η^2 = 0.863; a significant main effect for distribution of GCPs, F (2,45) = 25.018, p = <. 001, partial η^2 = 0.625; and significant interaction between number and distribution of GCPs, F (8, 45) = 4.503, p = .001, partial η^2 = 0.546. Post hoc analysis (Table 9) using Tukey's HSD for the main effect revealed that vertical accuracy was marked higher for 16 and 20 GCPs, followed by 8 and 12 GCPs, the lowest vertical accuracy observed for 4 GCPs.

Table 7: Descriptive Statistics of transformed vertical accuracy

Number of GCPs	GCPs distribution	Mean (cm)	SD (cm)
4	Outer	184.63	50.09
	Center	144.89	16.45
	Stratified	158.58	15.86
8	Outer	57.79	90.91
	Center	106.33	64.46
	Stratified	54.16	91.98
12	Outer	59.87	20.24
	Center	113.87	93.88
	Stratified	31.68	17.45
16	Outer	-2.47	36.53
	Center	84.23	9.83
	Stratified	-1.36	11.49
20	Outer	-15.12	44.17
	Center	87.80	3.73
	Stratified	9.09	34.38

Table 8: Summary of ANOVA table for vertical accuracy

Source	*Df*	*MS*	*F*	*P*	Effect Size
Number of GCPs	4	2.764	47.364	<.001	.863
Distribution of GCPs	2	1.460	25.018	<.001	.625
Number* Distribution	8	.263	4.503	.001	.546
Total	45				

Note: MS = Mean squares, effect size = η^2 or partial η^2

Table 9: Tukey post hoc test of vertical accuracy

Number of GCP	Vertical accuracy (cm)			Mean (cm)
	Outer	Center	Stratified	
4	169.10^{A}	165.50^{A}	168.80^{A}	167.80^{a}
8	20.80^{D}	117.60^{B}	19.60^{D}	52.70^{b}
12	24.80^{D}	134.10^{B}	14.90^{D}	57.90^{b}
16	11.90^{D}	63.20^{C}	11.60^{D}	28.90^{c}
20	11.50^{D}	73.30^{C}	12.60^{D}	32.50^{c}
Mean	47.60^{b}	110.80^{a}	45.50^{b}	70.50

Additionally, it was observed that vertical accuracy was significantly lower for the center distribution compared to both outer distributions and stratified distributions. In terms of the interaction, 8, 12, 16, and 20 GCPs exhibited significantly higher vertical accuracy than 4 GCPs. Furthermore, no significant difference was found in the vertical accuracy between GCPs arranged in outer and stratified setups, while center distributions of GCPs yielded less accurate vertical accuracy. Figure 7 shows the graph of number and spatial distribution of GCPs vs vertical accuracy, showing that as the number of GCPs increases from 4 to 20 both for outer and stratified distributions, the vertical accuracy increases from 169.10 cm for outer and 168.80 cm for stratified distribution to 11.50 cm for outer and 12.60 cm for stratified distributions.

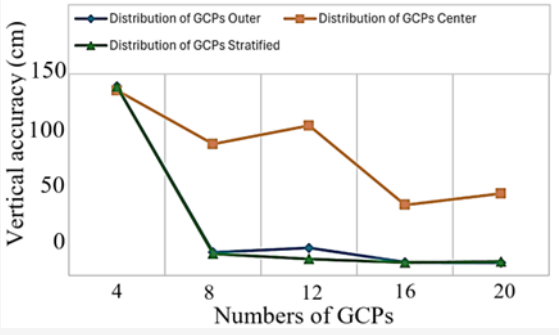

Figure 7: Number and Distribution of GCPs vs Vertical accuracy

The graph shows the overlapping of means of outer and stratified distribution confirming the findings of the ANOVA that there is a significant interaction between the number and distribution of GCPs. This means that as the number of GCPs increases, means of outer and stratified are statistically the same and not comparable to the means of the center distribution. For the center distribution, its vertical accuracy increases from 165.50 to 73.30 cm for 4 and 20 GCPS, respectively.

3.2 Horizontal Accuracy

Table 10 displays the dataset for horizontal accuracy in a 5 x 3 factorial design of experiments, incorporating 5 levels of the number of GCPs and 3 levels of the distribution of GCPs. Figure 8 illustrates the probability of normal distribution. Additionally, Table 11 presents the normality test results using Kolmogorov-Smirnov and Shapiro-Wilk tests, indicating p-values greater than 0.05. This suggests that the data adheres to a normal distribution. A two-way ANOVA was performed to evaluate the effects of number and distribution of GCPs on horizontal accuracy of the UAV Orthomosaic map. The means and standard deviations for horizontal accuracy of the UAV Orthomosaic map are presented in Table 12.

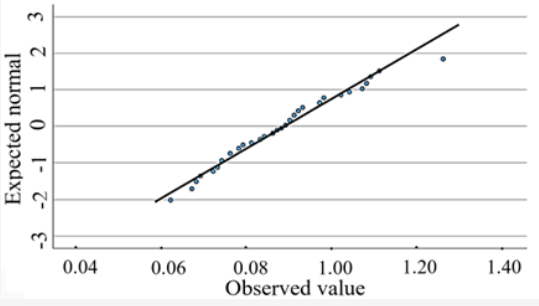

Figure 8: Normal Q-Q plot of horizontal accuracy

Table 10: Horizontal accuracy

Number of GCPs	Horizontal accuracy (cm)		
	Outer	Center	Stratified
4	9.20	12.60	8.30
	7.20	10.80	8.40
	10.80	10.70	10.20
8	8.10	12.60	8.80
	9.00	11.10	6.70
	9.80	9.70	7.80
12	9.10	9.10	10.90
	8.60	8.90	7.60
	7.80	9.20	7.60
16	7.40	7.40	6.90
	9.70	9.30	8.90
	10.40	8.30	9.70
20	8.60	8.70	7.90
	7.30	9.00	6.80
	6.20	9.00	7.40

Table 11: Test of normality of horizontal accuracy

	Kolmogorov-Smirnov			Shapiro-Wilk		
	Stat.	df	Sig.	Stat.	df	Sig.
Vertical Accuracy	.102	45	.200	.966	45	.208

Table 12: Descriptive statistics of horizontal accuracy

Number of GCPs	GCPs Distribution	Mean (cm)	SD (cm)
4	Outer	9.10	1.80
	Center	11.40	1.10
	Stratified	9.00	1.10
8	Outer	9.00	0.90
	Center	11.10	1.50
	Stratified	7.80	1.10
12	Outer	8.50	0.70
	Center	9.10	0.20
	Stratified	8.70	1.90
16	Outer	9.20	1.60
	Center	8.30	1.00
	Stratified	8.50	1.40
20	Outer	7.40	1.20
	Center	8.90	0.20
	Stratified	7.40	0.60

The results in Table 13 indicated significant main effect of number of GCPs, $F(4, 45) = 3.377$, $p = .021$, partial $\eta^2 = .310$; a significant main effect for distribution of GCPs, $F(2,45) = 6.660$, $p = .004$, partial $\eta^2 = .307$; and no significant interaction between number of GCPs and distribution of GCPs, $F(8, 45) = 1.484$, $p = .205$, partial $\eta^2 = .284$. Post hoc testing using Tukey's HSD is presented in Table 14, indicating that horizontal accuracy was significantly highest for 20 number of GCPs, 4, 8, 12 and 16 number of GCPs will have the same effect on the horizontal accuracy. Also indicated that horizontal accuracy was significantly lower for center distribution than for both outer distributions and stratified distributions. Figure 9 illustrates the relationship between the number and spatial distribution of (GCPs) vs horizontal accuracy.

Table 13: Summary of ANOVA table for horizontal accuracy

Source	*Df*	*MS*	*F*	*P*	*Effect Size*
Number of GCPs	4	.000	3.377	.021	.310
Distribution of GCPs	2	.001	6.660	.004	.307
Number* Distribution	8	.000	1.484	.205	.284
Total	45				

Note: MS = Mean squares, effect size = η^2 or partial η^2

Table 14: Tukey post hoc test of horizontal accuracy

Number of GCP	Horizontal accuracy (cm)			Mean (cm)
	Outer	Center	Stratified	
4	9.10	11.40	9.00	9.80[a]
8	9.00	11.10	7.80	9.30[ab]
12	8.50	9.10	8.70	8.80[ab]
16	9.20	8.30	8.50	8.70[ab]
20	7.40	8.90	7.40	7.90[b]
Mean	8.60[b]	9.80[a]	8.30[b]	8.90

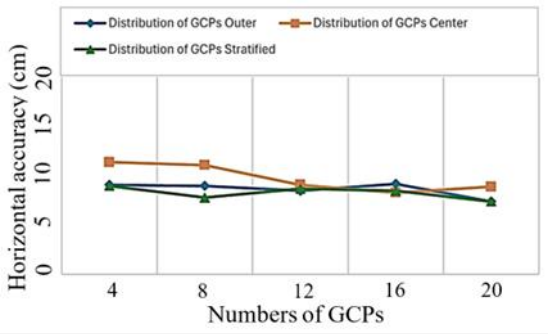

Figure 9: Number and distribution of GCPs vs horizontal accuracy

Despite observing a crisscrossing of means, particularly at 4, 12 and 16 GCPs for all distributions, the ANOVA indicates that this interaction is not statistically significant, as reflected by a p-value of 0.205 which implies that the horizontal accuracy will consistently follow a parallel trend with an increasing number of GCPs, regardless of distribution. The trend of horizontal accuracy is increasing as the number of GCPS increases for all distributions. The main effect of both number and spatial distribution of GCPs are significant which means among each independent variables there are differences in the effect on horizontal accuracy. The number of GCPs, specifically 4, 8, 12, and 16, exhibit similarities among themselves but differ significantly from the set of 20 GCPs. The outer and stratified effects are statistically equivalent, contrasting with the impact of the center distribution, which proves to be less accurate.

3.3 Discussion on Vertical and Horizontal Accuracy

The current investigation yielded a vertical accuracy range of 11.50 to 169.10 cm and a horizontal accuracy range of 7.40 to 11.40 cm. Employing 8, 12, 16, and 20 GCPs arranged in both outer and stratified distributions demonstrated comparable performance, achieving the highest vertical accuracy within the range of 11.50 to 24.80 cm. The utilization of 4 GCPs resulted in a mean vertical accuracy of 167.80 cm across all distributions.

The highest horizontal accuracy of 7.40 cm was achieved with 20 GCPs arranged in an outer and stratified distribution. Following this, 4, 8, 12, and 16 GCPs arranged in outer and stratified distributions exhibited horizontal accuracies ranging from 8.30 to 11.40 cm. In contrast, a previous study [32] reported vertical accuracies ranging from 78.00 to 83.00 cm and horizontal accuracies from 46.00 to 49.00 cm, which were less precise than those in the present study. This difference is attributed to the larger study area of 150 ha in the previous work [32], leading to lower GCP densities compared to the 100 ha area in the current study. The increasing trend observed in both vertical and horizontal accuracy aligns with findings from previous studies, which emphasize the positive impact of increasing the number of GCPs on accuracy [32] [33] [31] [24] [29] [38] and [39]. Notably, the horizontal accuracy (7.40 to 11.40 cm) surpassed the vertical accuracy (11.50 to 169.10 cm), consistent with the findings of the previous study [29] [32] and [39]. Among the tested GCP distributions, the outer and stratified configurations consistently yielded the best vertical and horizontal accuracy, aligning with findings from previous studies [24] and [29].

Despite the mixed land use and vegetation within the study area, the classification achieved for NVA in terms of vertical accuracy, using 8, 12, 16, and 20 ground control points (GCPs) arranged in both outer and stratified distributions and falling within the range of 11.50 to 24.80 cm, is designated as the 20-cm Vertical Class according to the ASPRS Positional Accuracy Standards for Digital Geospatial Data of 2023 [37]. The ASPRS Positional Accuracy Standards for Digital Geospatial Data in 2023 stipulate that in vegetated areas, the specified vertical accuracy will be acknowledged but will not serve as a pass/fail criterion for the project. While all horizontal accuracy obtained in the present study regardless of distribution falls on the 10-cm Horizontal Class in the ASPRS Positional Accuracy Standards for Digital Geospatial Data of 2023 [37].

4. Conclusions

This study aimed to identify the most effective GCP configuration for the UAV-based DEM, specifically focusing on achieving optimal accuracy in DEMs. It was achieved by discussing the impact of the different number and spatial distribution of GCPs on both vertical and horizontal accuracy of UAV-based DEMs. Enhanced DEMs accuracy translates to increased precision when applying this UAV-based DEM in geohazard scenarios such as flood modeling. The summary of the findings was the following:

1. Vertical accuracy of UAV-based DEM is greatly affected by the number and spatial distribution of GCPs
2. As the number of GCPs increases, the vertical accuracy of the UAV-based DEM increases
3. Outer and stratified distribution of GCPs produced same effect on the vertical accuracy of UAV-based DEM and more accurate compared with center distribution of GCPs
4. Eight (8), 12, 16 and 20 number of GCPs arranged in either outer or stratified distributions will have the same effect on the vertical accuracy of the UAV-based DEM and more accurate than with 4 number of GCPs regardless of distribution
5. Horizontal accuracy of UAV-based DEM is affected by the number and spatial distribution of GCPs
6. Number of GCPS 4, 8, 12, and 16 will have the same effect on the horizontal accuracy of UAV-based DEM
7. Twenty (20) number of GCPs will give the most accurate UAV-based DEM in terms of horizontal accuracy
8. The study produced a 20-cm Vertical Accuracy Class and 10-cm Horizontal Accuracy Class based on ASPRS Positional Accuracy Standards for Digital Geospatial Data of 2023

Setting up GCPs for UAV-based DEM is often time-consuming, labor-intensive, and costly. Understanding the optimal number and distribution of GCPs can significantly reduce these challenges, allowing projects to be completed with minimal effort while maintaining acceptable accuracy. This is particularly important in difficult survey areas, such as mountainous or unstable slopes, as well as in urban environments where obstructions are common. This study identified the optimal GCP configuration for UAV-based DEM, recommending the use of either an outer or stratified distribution of GCPs. If a stratified arrangement is not feasible, an outer distribution can be substituted, or vice versa, without compromising UAV-based DEM accuracy. Based on the findings, it is concluded that the best results for UAV-based DEMs can be achieved by using eight (8) GCPs per 1 km² (or 100 hectares), arranged in either an outer or stratified pattern.

References

[1] Gacu, J. G., Monjardin, C. E. F., Senoro, D. B. and Tan, F. J., (2022). Flood Risk Assessment Using GIS-Based Analytical Hierarchy Process in the Municipality of Odiongan, Romblon, Philippines. *Applied Sciences*, Vol. 12(19), 9456-9487. https://doi.org/10.3390/app12199456.

[2] Hariyono, M. I. and Kurniawan, A. A., (2022). The Use of Digital Elevation Model in a GIS for Flood Vulnerability: Case Study of Sitiarjo Village Malang District East Java Indonesia. *IOP Conference Series: Earth and Environmental Science*, Vol. 1039. https://doi.org/10.1088/1755-1315/1039/1/012020.

[3] Kumar, V., Sharma, K., Caloiero, T., Mehta, D. and Singh, K., (2023). Comprehensive Overview of Flood Modeling Approaches: A Review of Recent Advances. *Hydrology*, Vol. 10(7), 141-162. https://doi.org/10.3390/hydrology10070141.

[4] Lakshmi, S. E. and Yarrakula, K., (2018). Review and Critical Analysis of Digital Elevation Models. *Geofizika*, Vol. 35(2), 129–157. https://doi.org/10.15233/gfz.2018.35.7.

[5] Xu, K., Fang, J., Fang, Y., Sun, Q., Wu, C. and Liu, M., (2021). The Importance of Digital Elevation Model Selection in Flood Simulation and a Proposed Method to Reduce DEM Errors: A Case Study in Shanghai. *International Journal of Disaster Risk Science*, Vol. 12(6), 890–902. https://doi.org/10.1007/s13753-021-00377-z.

[6] Saksena, S. and Merwade, V., (2015). Incorporating the Effect of DEM Resolution and Accuracy for Improved Flood Inundation Mapping. *Journal of Hydrology*, Vol. 530, 180–194. https://doi.org/10.1016/j.jhydrol.2015.09.069.

[7] Yamazaki, D., Ikeshima, D., Tawatari, R., Yamaguchi, T., O., Loughlin, F., Neal, J. C., Sampson, C., Kanae, S. and Bates, P. D., (2017). A High‐Accuracy Map of Global Terrain Elevations. *Geophysical Research Letters*, Vol. 44(11), 5844-5853. https://doi.org/10.1002/2017gl072874.

[8] Polat, N. and Uysal, M., (2015). Investigating Performance of Airborne LiDAR Data Filtering Algorithms for DTM Generation. *Measurement*, Vol. 63, 61–68. https://doi.org/10.1016/j.measurement.2014.12.017.

[9] Khalid, N. F., Din, A. H., Omar, K. M., Khanan, M. F., Omar, A. H., Hamid, A. I. and Pa'suya, M. F., (2016). Open-source Digital Elevation Model (DEM) Evaluation with GPS and LiDAR Data. *The International Archives of Photogrammetry, Remote Sensing and Spatial Information Sciences*, Vol. XLII-4/W1, 299–306. https://doi.org/10.5194/isprs-archives-xlii-4-w1-299-2016.

[10] Uysal, M., Toprak, A. S. and Polat, N., (2015). DEM Generation with UAV Photogrammetry and Accuracy Analysis in Sahitler Hill, *Measurement*, Vol. 73, 539–543. https://doi.org/10.1016/j.measurement.2015.06.010.

[11] Santillan, J. R. and Makinano-Santillan, M., (2016). Vertical Accuracy Assessment of 30-M Resolution ALOS, ASTER, and SRTM Global DEMs Over Northeastern Mindanao, Philippines. *The International Archives of Photogrammetry, Remote Sensing and Spatial Information Sciences*, Vol. XLI-B4, 149–156. https://doi.org/10.5194/isprs-archives-xli-b4-149-2016.

[12] Walczak, Z., Sojka, M., Wróżyński, R. and Laks, I., (2016). Estimation of Polder Retention Capacity Based on ASTER, SRTM and LiDAR DEMs: The Case of Majdany Polder (West Poland). *Water*, Vol. 8(6), 230-250. https://doi.org/10.3390/w8060230.

[13] Mukherjee, S., Joshi, P. K., Ghosh, A., Garg, R. D. and Mukhopadhyay, A., (2013). Evaluation of Vertical Accuracy of Open-source Digital Elevation Model (DEM). *International Journal of Applied Earth Observation and Geoinformation*, Vol. 21, 205–217. https://doi.org/10.1016/j.jag.2012.09. 004.

[14] Talchabhadel, R., Nakagawa, H., Kawaike, K., Yamanoi, K. and Thapa, B. R., (2021). Assessment of Vertical Accuracy of Open Source 30-m Resolution Space-borne Digital Elevation Models. *Geomatics, Natural Hazards, and Risk*, Vol. 12, 939–960. https://doi.org/10.1080/19475705.2021.1910575.

[15] Coveney, S. and Fotheringham, A. S., (2011). The Impact of DEM Data Source on Prediction of Flooding and Erosion Risk Due to Sea-level Rise. *International Journal of Geographical Information Science*, Vol. 25(7), 1191–1211. https://doi.org/10.1080/13658816.2010.545064

[16] Chonpatathip, S. (2023). Earthwork Volume Measurement in Road Construction Using Unmanned Aerial Vehicle (UAV). *International Journal of Geoinformatics*, Vol. 19(12), 51–64. https://doi.org/10.52939/ijg.v19i12.2977.

[17] Chonpatathip, S., Suanpaga, W., and Chantawarangul, K. (2023). Utilizing Unmanned Aerial Vehicles (UAVs) for Earthwork Fill Height Determination in Road Construction. *International Journal of Geoinformatics*, Vol. 19(10), 28–39. https://doi.org/10.52939/ijg.v19i9.2877.

[18] Zhang, Z. and Zhu, L., (2023). A Review of Unmanned Aerial Vehicle Remote Sensing: Platforms, Sensors, Data Processing Methods, and Applications. *Drones*, Vol. 7(6), 398-440. https://doi.org/10.3390/drones7060398.

[19] Jiménez-Jiménez, S. I., Ojeda-Bustamante, W., Marcial-Pablo, M. and Enciso, J., (2021). Digital Terrain Models Generated with Low-Cost UAV Photogrammetry: Methodology and Accuracy. *ISPRS International Journal of Geo-Information*, Vol. 10(5), 285-322. https://doi.org/10.3390/ijgi10050285.

[20] Yang, H., Bian, H., Li, B., Bi, W. and Zhao, X., (2022). A Low-Cost and Ultralight Unmanned Aerial Vehicle-Borne Multicamera Imaging System Based on Smartphones. *Mathematical Problems in Engineering*, Vol. 2022, 1–15. https://doi.org/10.1155/2022/8524400.

[21] Yao, H., Qin, R. and Chen, X., (2019). Unmanned Aerial Vehicle for Remote Sensing Applications-A Review. *Remote Sensing*, Vol. 11(12), 1443-1465. https://doi.org/10.3390/rs11121443.

[22] Szypuła, B., (2023). Accuracy of UAV-Based DEMs without Ground Control Points. *GeoInformatica*, Vol. 28, 1–28. https://doi.org/10.1007/s10707-023-00498-1.

[23] Escobar Villanueva, J. R., Iglesias Martínez, L. and Pérez Montiel, J. I., (2019). DEM Generation from Fixed-Wing UAV Imaging and LiDAR-Derived Ground Control Points for Food Estimations. *Sensors*, Vol. 19(14), 3205-3225. https://doi.org/10.3390/s19143205.

[24] Thanh, P., Elshewy, M., Long, N. and Thom, T., (2023). Creation and Assessment of a Topographic Map from Unmanned Aerial Vehicle Data in Thanh Son District, Vietnam. *International Journal of Geoinformatics*, Vol. 19(3), 57–66. https://doi.org/ 10.52939/ijg.v19i3.2605.

[25] Sanz-Ablanedo, E., Chandler, J. H., Rodríguez-Pérez, J. R. and Ordóñez, C., (2018). Accuracy of Unmanned Aerial Vehicle (UAV) and SfM Photogrammetry Survey as a Function of the Number and Location of Ground Control Points Used. *Remote Sensing*, Vol. 10(10), 1606-1625. https://doi.org/10.3390/rs10101606.

[26] Zeybek, M., (2021). Accuracy Assessment of Direct Georeferencing UAV Images with Onboard Global Navigation Satellite System and Comparison of CORS/RTK Surveying Methods. *Measurement Science and Technology*, Vol. 32(6). https://doi.org/10.1088/1361-6501/abf25d.

[27] Son, S. W., Yoon, J. H., Jeon, H. J., Kim, D. W. and Yu, J. J., (2019). Optimal Flight Parameters for Unmanned Aerial Vehicles Collecting Spatial Information for Estimating Large-Scale Waste Generation. *International Journal of*

Remote Sensing, Vol. 40(20), 8010–8030. https://doi.org/10.1080/01431161.2019.1608387.

[28] Coveney, S. and Roberts, K., (2017). Lightweight UAV Digital Elevation Models and Ortho-imagery for Environmental Applications: Data Accuracy Evaluation and Potential for River Flood Risk Modelling. *International Journal of Remote Sensing*, Vol. 38(8–10), 3159–3180. https://doi.org/10.1080/01431161.2017.1292074.

[29] Villanueva, J. K. and Blanco, A. C., (2019). Optimization of Ground Control Point (GCP) Configuration for Unmanned Aerial Vehicle (UAV) Survey Using Structure from Motion (SFM). *The International Archives of Photogrammetry, Remote Sensing and Spatial Information Sciences*, Vol. XLII-4/W12, 167–174. https://doi.org/10.5194/isprs-archives-xlii-4-w12-167-2019.

[30] Oniga, V. E., Breaban, A. I., Pfeifer, N. and Chirila, C., (2020). Determining the Suitable Number of Ground Control Points for UAS Images Georeferencing by Varying Number and Spatial Distribution. *Remote Sensing*, Vol. 12(5), 876-899. https://doi.org/10.3390/rs12050876.

[31] Agüera-Vega, F., Carvajal-Ramírez, F. and Martínez-Carricondo, P., (2017). Accuracy of Digital Surface Models and Orthophotos Derived from Unmanned Aerial Vehicle Photogrammetry. *Journal of Surveying Engineering*, Vol. 143(2). https://doi.org/10.1061/(asce)su.1943-5428.0000206.

[32] Tahar, K. N., (2013). An Evaluation on Different Number of Ground Control Points in Unmanned Aerial Vehicle Photogrammetric Block. *The International Archives of Photogrammetry, Remote Sensing and Spatial Information Sciences*, Vol. XL-2/W2, 93–98. 2013. https://doi.org/10.5194/isprsarchives-xl-2-w2-93-2013.

[33] Tonkin, T. and Midgley, N., (2016). Ground-Control Networks for Image Based Surface Reconstruction: An Investigation of Optimum Survey Designs using UAV Derived Imagery and Structure-from-Motion Photogrammetry. *Remote Sensing*, Vol. 8(9), 786-794. https://doi.org/10.3390/rs8090786.

[34] Liu, X., Lian, X., Yang, W., Wang, F., Han, Y. and Zhang, Y., (2022). Accuracy Assessment of a UAV Direct Georeferencing Method and Impact of the Configuration of Ground Control Points. *Drones*, Vol. 6(2), 30-45. https://doi.org/10.3390/drones6020030.

[35] Sampson, C., Smith, A., Bates, P., Neal, J. and Trigg, M., (2016). Perspectives on Open Access High Resolution Digital Elevation Models to Produce Global Flood Hazard Layers. *Frontiers in Earth Science*, Vol 3(85). https://doi.org/10.3389/feart.2015.00085.

[36] Verhoeven, G. J., (2010). It's All About the Format – Unleashing the Power of Raw Aerial Photography. *International Journal of Remote Sensing*, Vol 31(8), 2009–2042. https://doi.org/10.1080/01431160902929271.

[37] ASPRS, (2023). Positional Accuracy Standards for Digital Geospatial Data. *Photogrammetric Engineering & Remote Sensing*, Vol. 89(10), 589–592. https://doi.org/10.14358/pers.89.10.589.

[38] Ren, H., Zhao, Y., Xiao, W., Wang, X. and Sui, T., (2020). An Improved Ground Control Point Configuration for Digital Surface Model Construction in a Coal Waste Dump Using an Unmanned Aerial Vehicle System. *Remote Sensing*, Vol. 12(10), 1623-1638. https://doi.org/10.3390/rs12101623.

[39] Ulvi, A., (2021). The Effect of the Distribution and Numbers of Ground Control Points on the Precision of Producing Orthophoto Maps with an Unmanned Aerial Vehicle. *Journal of Asian Architecture and Building Engineering*, Vol. 20(6), 806–817. https://doi.org/10.1080/13467581.2021.1973479.